Cerebellar contribution to preparatory activity in motor neocortex

Francois Chabrol, Antonin Blot and Thomas D. Mrsic-Flogel

Biozentrum, University of Basel, Klingelbergstrasse 70, 4056 Basel, Switzerland.

Sainsbury Wellcome Center, University College London, 25 Howland Street London, W1T 4JG, UK.

Correspondence: t.mrsic-flogel@ucl.ac.uk; f.chabrol@ucl.ac.uk

In motor-related areas of the neocortex, preparatory neuronal activity predictive of specific actions emerges seconds in advance of movement and is maintained by a positive feedback loop with the thalamus. A major source of excitatory drive to the motor thalamus is the cerebellum, which has been implicated in coordination and timing of learned actions. However, the cerebellar contribution to neocortical signals coupled to movement planning remains poorly understood. Here we show that cerebellar output neurons in the dentate nucleus exhibit preparatory ramping activity in anticipation of expected rewards in a virtual reality conditioning task, a profile similar to that recorded in anterolateral motor neocortex (ALM). The preparatory activity in the dentate nucleus is controlled by a disinhibitory circuit involving inhibitory Purkinje cells in the cerebellar cortex, many of which suppress their firing in advance of rewards. Silencing the activity in the dentate nucleus by photoactivation of Purkinje cells caused robust, short-latency suppression in the majority of ALM neurons exhibiting preparatory activity. Thus, preparatory signals in motor neocortex require the output of the cerebellum. We suggest that the reciprocal circuitry between neocortex and cerebellum generates the sequence of activity required for planning and temporal coordination of learned, goal-directed actions.

The cerebellum is a key brain structure for the learning of sensorimotor and internal context relevant for movement timing[1]. The cerebellar hemispheres are interconnected with the neocortex via the disynaptic cortico-ponto-cerebellar and cerebello-thalamo-cortical pathways[2–6]. The sole output of the cerebellum are the deep cerebellar nuclei, where ~40 inhibitory Purkinje cells converge on individual postsynaptic cells[7]. The dentate nucleus (DN), the most lateral output nucleus of the cerebellum, sends excitatory projections to the motor thalamic regions linked to cortical areas involved in the preparation and execution of voluntary movements[8–12]. Although the cerebellum is mostly known for its role in adjusting the timing and degree of muscle activation, neurons at different stages of cerebellar hierarchy can also encode signals related to upcoming movements or salient events such as reward[13–16]. For

instance, DN neurons exhibit ramping activity predictive of the timing and direction of the self-initiated saccades[17,18]. Although these results suggest that the cerebellum participates in programming future actions, its contribution to preparatory activity in the neocortex during goal-directed behaviour remains to be determined.

We developed a visuomotor task in which mice ran through a virtual corridor comprising salient visual cues to reach a defined location where a reward was delivered (**Fig. 1a,b**; see Methods). Within a week of training, mice learned to estimate the reward location from visual cues, and adjusted their behaviour accordingly, by running speedily through the corridor before decelerating abruptly and licking upon reward delivery (**Fig. 1c-e,** Extended Data Fig. 1a-c). This behavioural progress was apparent during each session, as the number of false alarm licks outside of the reward zone decreased within tens of trials (Extended Data Fig. 1d), while deceleration and lick onsets emerged in anticipation of reward (**Fig. 1c-e**; Extended Data Fig. 1e).

To identify a cerebellar region integrating visuomotor signals from the neocortex, we stimulated electrically the primary visual (V1) and limb motor cortex (lM1) while looking for hemodynamic signals over the dorsal surface of the lateral cerebellum (Extended Data Fig. 2). We found a region in the lateral part of Crus1 that uniquely responded to both activation of V1 and lM1. As Crus1 projects to the dentate nucleus (DN)[19,20], we used silicon probes to record spiking activity of cerebellar output neurons in the DN to assess the involvement of the visuomotor cerebellum during the task (**Fig. 1f**). We identified the neural correlates of running, licking, or reward context in the reward zone by applying a generalised linear model (GLM)[21] to classify DN neurons according to running speed, lick times, reward time, and visual cues (see Methods). Fifty percent of all recorded DN neurons (n = 362, 16 mice) could not be classified according to any of the task variables. The activity of 64% of classified DN neurons was related to reward time (**Fig. 1g**, see below). The activity of other neurons was related to lick times, running, or a mixture of either plus reward times, but none had activity associated with the visual cues (**Fig. 1g**).

Of neurons whose activity was modulated by reward timing, 16% of neurons (*n* = 17) ramped up their activity a few seconds before reward delivery and stopped firing abruptly thereafter (classified as 'type 1' neurons; see [22]; **Fig. 1i**); 32% of neurons (*n* = 36) exhibited activity modulation before and after reward delivery ('type 2'; **Fig. 1j**); 52% of neurons (*n* = 59) were active just after reward delivery ('type 3'; **Fig. 1k**). Accordingly, DN population activity tiled the time period around reward delivery (**Fig. 1l**). Cross-covariance analysis between firing rate and lick rate revealed that preparatory activity arises long before the time of the reward (**Fig. 1m**). Type 1 and type 2 neurons' spiking preceded lick rate by 750 and 650 ms, respectively, on average, while type 3 neurons' spiking lagged lick rate by 170 ms, on

average (**Fig. 1m,n**). Moreover, type 1 DN neuron activity was anti-correlated with running speed and led its changes by 1.1 s on average. (**Fig. 1o,p**).

To verify that the activity of type 1-3 DN neurons was specific to reward context (**Fig. 1q**), we examined whether their firing was directly related to changes in motor output or visual input. Specifically, their activity was not modulated by deceleration events (**Fig. 1r**) or licking bouts outside of the reward zone (**Fig. 1s**), nor by the appearance of non-rewarded checkerboards in a different segment of the virtual corridor (**Fig. 1t**). Instead type 1-3 DN neurons were mainly active around the time of reward delivery (**Fig. 1q-t**). Taken together, these results suggest that DN neurons encode reward time-related information or actions plans required for obtaining reward.

To gain insight in how ramping activity could emerge in DN neurons that are under the control of the cerebellar cortex, we recorded from putative inhibitory Purkinje cells (PCs) in lateral Crus1 (**Fig. 2a,b**). The firing of PCs was modulated on the same time scale around the time of reward delivery as simultaneously recorded DN neurons (**Fig. 2c-n**). However, the majority of PCs ramped down their activity prior to reward (**Fig. 2p**), while DN neurons exhibited both activity increases or decreases (**Fig. 2o**). Accordingly, the average z-score of PC firing in the last second preceding reward was negative (-0.14 +/- 0.35, n = 83, $p < 0.0001$), in contrast to DN neurons (0.05 +/- 0.51, n = 77, p = 0.4, PC vs DN: p = 0.0007, **Fig. 2q**). PCs provide inhibitory synapses onto DN neurons. To test if the recorded regions of Crus I and DN were directly connected, we computed the cross-correlogram between all pairs of simultaneously recorded neurons. A small fraction of these correlograms showed significant modulation (56/2163, see Methods), on average exhibiting a millisecond-latency trough, consistent with monosynaptic inhibition from PC to DN neurons (**Fig. 2r**). Over longer timescale, individual pairs often displayed large negative cross-covariance (**Fig. 2s**, see Methods), indicating that cells are anti-correlated. The average cross-covariance between all pairs measured before the reward (**Fig. 2t**) revealed that PC activity preceded suppression of DN neuron responses at a lag of ~550ms. Thus the ramping down of PC activity may relieve DN neurons of inhibition and allow extra-cerebellar inputs (ref) to drive the ramping activity in anticipation of reward.

The firing profiles observed in DN were reminiscent of activity patterns recorded in motor-related areas of neocortex during movement planning and execution[22]. Specifically, the pre-reward ramping activity of type 1 and type 2 DN neurons closely resembled preparatory activity of neurons in ALM, which become active as mice prepare for licking[23]. Furthermore, their activity strongly resembles that of DN neurons in primates that have been shown to control the preparation and timing of voluntary saccades[17,18]. Given the substantial lead times of type 1 and some type 2 DN neuron activities over lick

rate and running speed changes, these neurons might encode the conjunction of reward anticipation and motor plans, and thus contribute to motor preparation for licking to the upcoming reward.

Since DN neurons project to ventral thalamus[8,11,12,24], which has been shown to participate in the maintenance of preparatory activity in mouse ALM neocortex[24]. Since DN neurons project to ventral thalamus[8,11,12,24], which has been shown to participate in the maintenance of preparatory activity in mouse ALM neocortex[24], we investigated whether DN activity could influence ALM processing. We first verified whether ALM neurons were engaged during our behavioural task, especially during the transition period between running and licking around reward delivery (**Fig. 3a,b**). The activity of 51% of putative ALM pyramidal cells (see Methods) was correlated with task variables according to GLM (n = 147/288, 4 mice). We found that the activity of 86% of those units was related to reward time, including neurons with ramping activity a few seconds before reward delivery which terminated abruptly thereafter (classified as 'type 1', n = 16, **Fig. 3f,c,g**), neurons active before and after reward delivery ('type 2', n = 42, **Fig. 3f,dg**), or neurons active after reward delivery ('type 3', n = 66, **Fig. 3f,e,g**), consistent with previous reports in ALM[22]. Type 1-3 neuronal activity in ALM substantially co-varied with lick rate (**Fig. 3h**) and preceded it by 840, 500, and 240 ms on average (**Fig. 3i**). Moreover, type 1-2 neuronal activity also preceded running speed changes (**Fig. 3j**), albeit with anti-correlation, by 1170 ms and 200 ms on average, respectively (**Fig. 3k**). Finally, type 1-3 ALM neurons were not modulated by changes in motor behaviour or visual input outside of the reward zone (**Fig. 3l-o**). Thus, the temporal profiles of neuronal firing in ALM and their relationship to motor behaviour were similar to the majority of neurons in DN (**Fig. 1**).

To determine the contribution of DN firing on ALM preparatory activity, we silenced DN output by photoactivating cerebellar PCs expressing channelrhodopsin-2 under the control of the specific Purkinje cell protein (PCP2) promoter (**Fig. 4a,** see Methods). The activation of PCs in lateral Crus 1 was set to begin at 20 cm distance before the reward position in the virtual corridor (**Fig. 1b**) to occur approximately 1 s before reward and to terminate around reward delivery. Simultaneous silicone probe recordings from DN and ALM (**Fig. 4a**) revealed that optogenetic activation of PCs effectively silenced most DN neurons (**Fig. 4b**; Extended Data Fig. 3a) regardless of response type (**Fig. 4l,m,** firing rate control vs PC photoactivation: 43.56 +/- 30.57 Hz vs 8.08 +/- 21.06 Hz, 81 % decrease, $p < 0.0001$, n = 47, 3 mice). PC photoactivation also robustly suppressed activity in a large fraction of ALM neurons (n = 72/189, 3 mice; **Fig 4c-k,n,o**; Extended Data Fig. 3b). Most type 1 and type 2 neurons were robustly suppressed by PC photoactivation (respectively, 10/12 and 30/43 cells, **Fig. 4c,d,n**), such that, on average, their firing rate decreased to baseline activity levels (Type 1 control: 17.31 +/- 14.95 Hz vs

129 photoactivation: 10.10 +/- 13.10 Hz, *n* = 12, *p* = 0.0005; Type 2 control: 20.44 +/- 16.40 Hz vs
130 photoactivation: 11.15 +/- 11.66 Hz, *n* = 43, *p* < 0.0001, **Fig. 4h,i,o**), respectively. Type 3 and unclassified
131 ALM neurons exhibited a mixture of effects, including a fraction of units that were excited (**Fig. 4e,p**),
132 and their population activity during PC photoactivation remained unaffected on average (respectively
133 8.06 +/- 8.47 Hz vs 6.97 +/- 8.94 Hz, *p* = 0.06, *n* = 38 and 10.60 +/- 11.79 Hz vs 10.65 +/- 12.30 Hz, *p* =
134 0.7, *n* = 96, **Fig. 4j,k,n,o**). In trials with PC photoactivation, mice transiently decreased their running
135 speed approximately 150 ms after light onset (**Fig. 4f**, curve; Extended Data Fig. 3c), reaching the reward
136 later (**Fig. 4f**, histograms) and licking at that time (**Fig. 4g**). As Type 3 cells were modulated by reward
137 their firing peaked later in photoactivation trials (**Fig. 4j**) but remained aligned to reward delivery
138 (Extended Data Fig. 4). The inhibition of neuronal activity was not a consequence of running speed
139 change because the onset of the firing rate decrease was almost immediate in DN neurons (3 ms, see
140 Methods), and was 9 ms for type 1 and 2 ALM neurons (**Fig. 4q,r**), and a significant decrease in ALM
141 activity during PC photoactivation was observed before any change in running speed (10-120 ms from
142 photoactivation onset; Type 1 control: 17.37 +/- 14.74 Hz vs photoactivation: 12.00 +/- 13.57, *n* = 12, *p* =
143 0.001; Type 2 control: 18.84 +/- 15.15 Hz vs photoactivation: 14.55 +/- 13.57, *n* = 43, *p* = 0.0002; control
144 running speed: 17.1 +/- 6.7 cm/s vs photoactivation 17.8 +/-6.1;, p = 0.17; Extended Data Fig. 3c).
145 Moreover, the persistence of decreased activity in type 1 and 2 ALM neurons during the photoactivation
146 period could not be explained by the decrease in running speed as their activity is not affected by mouse
147 deceleration outside of the reward zone (**Fig. 1r**). The short-latency suppression of ALM activity was
148 consistent with the time delay expected for the withdrawal of excitation via the disynaptic pathway
149 from DN to ALM via the thalamus. The existence of ALM neurons that increased their activity following
150 PC activation (30/100, **Fig. 4p**) suggests an additional feedforward inhibitory circuit. Together, these
151 data indicate that DN provides preferential drive to the majority of ALM neurons exhibiting preparatory
152 activity (type 1 and type 2 cells). We suggest that the maintenance of preparatory activity in ALM
153 requires short-latency, excitatory feedback from the cerebellum.

154 Our results reveal the key contribution of the cerebellum in the generation of activity in the
155 neocortex that emerges in anticipation of reward delivery. The dentate nucleus exhibits preparatory
156 signals prior to reward that resemble those in the neocortex during motor preparation (**Fig. 1 & 3**; see
157 also[22,25,26]). Silencing dentate activity by photoactivation of Purkinje cells in cerebellar cortex caused a
158 short-latency suppression of the majority of ALM neurons exhibiting preparatory activity. This result is
159 consistent with observations that the dentate nucleus provides direct excitatory input to the
160 thalamus[8,10–12], which itself is essential for the maintenance of persistent activity in the neocortex[24,27,28]

Thus, the cerebellum has a specific and fast driving influence on motor cortex activity in anticipation of goal-directed actions.[8,10–12]. Thus, the cerebellum has a specific and fast driving influence on motor cortex activity in anticipation of goal-directed actions. Our data are in agreement with results from human case studies which propose that the cerebellum is a crucial component of a circuit involving motor thalamus and neocortex in the preparation of self-timed movements[29,30].

The cerebellum is known for its remarkable ability to learn the fine-scale temporal associations between internal and external context and specific actions[1,31,32]. We suggest that the preparatory activity originating within motor-related areas of the neocortex is conveyed to the cerebellum via the cortico-pontine-mossy fiber pathway where it may be combined with reward prediction signals[15] to adjust the timing of activity in preparation of goal-directed movements. The activity of Purkinje cells and dentate neurons is consistent with this hypothesis; a large fraction Purkinje cells decreased their activity in anticipation of reward, potentially shaping the ramping rate of preparatory activity in DN which peaks at the time of reward delivery. Thus, while preparatory signals may originate in the neocortex, the cerebellum is a key component that contributes to the timing of anticipatory activity that is maintained in the thalamocortical loop.

Given that multiple closed-loop circuits have been identified between the subdivisions of cerebellum and the neocortex[4,10,11,33,34] we suggest that ALM and the lateral Crus 1-dentate cerebellar pathway constitutes one such circuit dedicated to the generation of precisely-timed preparatory activity. Moreover, the deep cerebellar nuclei that send excitatory projections to other thalamic regions sub-serving non-motor cortical areas[4,10,11] may contribute to the maintenance of persistent neocortical activity during cognitive tasks requiring attention and working memory[35–37]. More generally, our data add to the growing body of evidence that persistent activity in the neocortex is not a result of recurrent neural interactions within local circuits, but instead requires the coordination of activity across distal brain regions[24,27,28].

Acknowledgements

We thank Mateo Velez-Fort and Francesca Greenstreet for help with experiments, and David Digregorio, Tom Otis, Marcus Stephenson-Jones and Petr Znamenskiy for constructive ideas and discussions about this work. The research was funded by the Biozentrum core funds, ERC Consolidator Grant and SNSF Project grant.

Author contributions

F.C. performed experiments. F.C. and A.B. analysed the data. All authors wrote the manuscript.

Methods

Animal care and housing. All experimental procedures were carried out in accordance with institutional animal welfare guidelines, and licensed by the Veterinary Office of the Canton of Basel, Switzerland. For this study we used 22 male C57BL6 mice (supplied by Janvier labs) aged > 60 days postnatal and 7 mice from a transgenic cross between Ai32(RCL-ChR2(H134R)/EYFP) and STOCK Tg(Pcp2-cre)1Amc/J lines. Animals were housed in a reverse 12:12 hour light/dark cycle and were food-restricted starting a week after surgery with maximum 20% weight loss. Surgical procedures were carried out aseptically on animals subcutaneously injected with atropine (0.1 mg kg^{-1}), dexamethasone (2mg kg^{-1}), and a general anesthetic mixed comprising fentanyl (0.05 mg kg^{-1}), midazolam (5mg kg^{-1}), and medetomidine (0.5mg kg^{-1}). Animals were injected an analgesic (buprenorphine, 0.1 mg kg^{-1}), and antibiotics (enrofloxacin, 5 mg kg^{-1}) at least 15 minutes prior to the end of the surgery and once every day for two days post-surgery. For intrinsic imaging mice were under 1-2% isoflurane anesthesia. For acute electrophysiological recordings mice were put under 1-2% isoflurane anesthesia during the craniotomy procedure and allowed to recover for 1-2 hours before recording.

Behaviour. Mice were trained for 1-2 weeks to run head-fixed on a Styrofoam cylinder in front of two computer monitors placed 22 cm away from the mouse eyes. Running speed was calculated from the tick count of an optical rotary encoder placed on the axis of the wheel with a Teensy USB development board, and was fed back as position to a Unity software to display visual flow of a virtual corridor using a MATLAB-based script. A reward delivery spout was positioned under the snout of the mouse from which a drop of soy milk was delivered at a defined position inside the corridor (at 360 cm from start). Licks were detected with a piezo disc sensor placed under the spout and signals were sent to the Teensy USB development board and extracted as digital signals. The virtual corridor was composed of a black and white random dot pattern on a grey background (80 cm long) followed by black and white checkerboard (40 cm long), black and white random triangle pattern on a grey background (80 cm long), vertical black and white grating (40 cm long), black and white random square pattern on a grey background (80 cm long), and a final black and white checkerboard inside which reward was delivered 40 cm from its beginning. Two seconds following reward delivery the mouse was allowed to move freely inside the virtual checkerboard pattern, after which the corridor was reset to the starting position. Mice were initially trained on a short version of the corridor (20, 10, 20, 10, 20 cm length for each visual pattern respectively, and reward position at 90 cm), before extending the corridor to full length in expert mice. Appearance of the visual patterns inside the virtual corridor was signalled by TCP when the mouse

reached the corresponding position in the virtual corridor. In 2/3 mice shown in **Figure 4**, the corridor started at 120 cm distance from start in order to increase the number of trials.

Virus and tracer injection. AAV2/1-Ef1a-eGFP-WPRE (30nl, $1.5e^{11}$ titre) was injected over 15-30 minutes with a *Toohey* Spritzer *Pressure System* (*Toohey Company*) with pulse duration from 5 to 20 milliseconds delivered at 1Hz with pressure between 5 and 15 psi into the left cerebellar crus 1 at the following coordinates: 6 millimetres posterior to Bregma, 3.3 mm Medio lateral, and at a depth of 200 µm. Two weeks after injection mice were euthanized with a dose of pentobarbital (80 mg kg^{-1}) and transcardially perfused with 4% paraformaldehyde. Perfused brains were put inside a block of agarose and sliced at 100 µm with a microtome. Slices were then mounted with a mixture of mounting medium and DAPI staining and imaged on a Zeiss LSM700 confocal microscope with a 40X oil objective.

Intrinsic signal imaging. Mice were anesthetized under 1-2% isoflurane and placed in a stereotaxic frame. A scalp incision was made along the midline of the head and the skull was cleaned and scraped. Two 80 µm tungsten wires (GoodFellow) were inserted inside polyimide tubes (230 µm O.D., 125 µm I.D.) and implanted 300 µm apart into the right primary visual (VisP) and limb motor cortex (lM1) following stereotaxic coordinates (2.7 posterior and 2.5 mm lateral to bregma, 0.25 anterior and 1.5 mm lateral to bregma, respectively) at 800 µm depth from the surface of the brain. Dental cement was added to join the wires to the skull. Neck muscles covering the bone over the cerebellum on the left side were gently detached and cut with fine scissors. The surface of the cerebellum was then carefully cleaned.

Animals were then placed inside a custom-built frame in order to incline the head and expose the surface of the bone above the cerebellum for imaging with a tandem lens macroscope. Mineral oil was applied to allow imaging through the bone. The mouse was lightly anaesthetized with 0.5-1% isoflurane and the body temperature monitored with an anal probe and maintained at 37°C. The preparation was illuminated with 700 nm light from an LED source and the imaging plane was focused 800 µm below the skull surface. Images were acquired through a bandpass filter centered at 700 nm with 10 nm bandwidth (Edmund Optics) at 6.25 Hz with a 12-bit CCD camera (1300QF; VDS Vosskülller) connected to a frame grabber (PCI-1422; National Instruments).

Tungsten wires were clamped with micro alligator clips and connected to a stimulus isolator (A395; World Precision Instruments). After a 10 s long baseline, trains of 700 µA stimuli were delivered at 6Hz with pulse duration of 200 µs for 3 s to each cortical area alternatively, followed by a 10 s long

recovery phase. Averages of 20 trials were calculated and hemodynamic signals were measured relative to the last 3 s before stimulation ($\Delta F/F_0$). Location of tungsten electrodes inside the neocortex were confirmed post-hoc with DiI labeling of the tracts.

Extracellular electrophysiology. Mice were anaesthetized according to the surgical procedure described in the animal care and housing section and placed into a stereotaxic frame. The skin over the skull was incised along the midline and the skull was cleaned and scrapped. A headplate was then attached to the skull in front of the cerebellum using Super Bond dental cement. For cerebellar recordings the neck muscles covering the bone were gently detached and cut with fine scissors on the left side. The surface of the skull over the cerebellum was then cleaned, a small piece of curved plastic was glued to the base of the exposed skull in order to support a well attached to the headplate and built up with dental cement and Tetric EvoFlow. The well was then filled with Kwik-Cast sealant. For the simultaneous recordings in cerebellum and ALM, a small additional well was built around stereotaxically-defined coordinates for the right ALM (2.3 mm anterior and 1.5 mm lateral to bregma).

On the day of the recording mice were anaesthetized under 1-2% isoflurane and small craniotomies (1mm diameter) were made above left lateral crus 1 (6 mm posterior and 3.3 mm lateral to bregma), left dentate nucleus (6 mm posterior, and 2.25 mm lateral to bregma), and/or right ALM (2.3 mm anterior and 1.5 mm lateral to bregma). Mice were allowed to recover from surgery for 1-2 hours before recording. Mice were then head-fixed over a Styrofoam cylinder. The well(s) around the craniotomy were filled with cortex buffer containing (in mM) 125 NaCl, 5 KCl, 10 Glucose monohydrate, 10 Hepes, 2 $MgSO_4$ heptahydrate, 2 $CaCl_2$ adjusted to pH 7.4 with NaOH. A silver wire was placed in the bath for referencing. Extracellular spikes were recorded using NeuroNexus silicon probes (A2x32-5mm-25-200-177-A64). The 64- or 128-channel voltages were acquired through amplifier boards (RHD2132, Intant Technologies) at 30 kHz per channel, serially digitized and send to an Open Ephys acquisition board via a SPI interface cable.

Photoactivation. A 200 µm diameter optical fiber was placed on top of the surface of lateral Crus1 using a manual micromanipulator. Light was delivered by a 100 mW 473 nm laser (CNI, MBL-III-473) triggered by a Pulse Pal pulse train generator (Open Ephys). To prevent mice from seeing the laser light, a masking 470 nm light from a fiber-coupled LED (Thorlabs) was placed in front of the connector between the patch cable and the optical fiber and turned on during the whole recording session. Mice were also trained in the presence of LED light. Black varnish was painted over the cement well surrounding the

craniotomy and black tape was wrapped around the connection between the patch cable and the optical fiber. One-second square light pulses (5 to 10 mW) were randomly delivered in 40 % of trials. Control trials from mice that experienced photoactivation were not included in **Figures 1-3** to avoid confounding effects such as plasticity-induced change in neuronal activity.

Electrophysiology data analysis.

Spikes were sorted with Kilosort (https://github.com/cortex-lab/Kilosort) using procedures previously described[38]. Briefly, the extracellular voltage recordings were high-pass filtered at 300 Hz, the effect of recording artifacts and correlated noise across channels were reduced using common average referencing and data whitening respectively. Putative spikes were detected using an amplitude threshold (4 s.d. of baseline) over the filtered voltage trace and matched to template waveforms. The firing rate for each unit was estimated by convolving a Gaussian kernel with spike times, σ was chosen according to the median inter-spike interval of each individual unit (**Fig. 1 & 2**). ALM units were classified as putative pyramidal neurons or fast-spiking interneurons based on spike width as described in[39].

For population scatter plots (**Fig. 1-3**) and averaging across neuronal activities grouped by type (**Fig. 1, 3**) we used the z-score of firing rates. For data plotted in **Figures 1q,s and 3l,n** the spike times of PCs and DN neurons were binned by 10 ms. The cross-covariance between firing rates of PC and DN pairs was then corrected for correlated firing resulting from stimulus effects by subtracting the cross-covariance between shuffled trials and was then normalized by the variance of the firing rates.

The cross-correlogram between each PC and DN cell simultaneously recorded (n = 2163 pairs, 3 mice) was computed with a bin of 1 ms (**Fig. 2r**). A correlogram was considered as modulated if at least two consecutive bins in the 20 ms following the Purkinje cell spike were above 3 std of the baseline computed in the [-50, -10] window. For all these pairs (56/2163) the cross-correlogram was z-scored by the mean/std of this baseline and all z-scored correlogram were averaged.

On longer time scale, task modulation of the cells entrains instabilities of the firing rate that might produce spurious covariance between co-modulated pairs. To assess the relation between PC activity and DN neuron activity on these time scale we used two equivalent methods. In **Figure 2s**, we used the cross-covariance as described above. In **Figure 2t**, the cross-correlogram between each pair was first calculated on each trial in the last 10 second before the reward (CC_{raw}). We then computed the cross-correlogram for the same pair but using trial n and n+1 ($CC_{shuffled}$). The shuffled corrected correlogram was then defined as ($CC_{raw} – CC_{shuffled}$) / sqrt($CC_{shuffled}$) and averaged across pairs.

ALM cells were considered modulated by cerebellar photoactivation if the average firing rate in the second following the onset of photostimulation was significantly (ranksum, alpha of 0.05) different from the average firing rate during the same window in control trials. We classified them as excited/inhibited if the control response was lower/higher than that during photoactivation trials. Average firing rate of the population in the same 1s window were compared between control and photoactivation condition using signrank test (alpha 0.05). Z-scored activity profiles were obtained for each cell by subtracting the average firing rate of the cell across the whole recording from the cell average activity profile in Hz and dividing it by the std of the firing rate. The z-scored activity profiles were then averaged together to generate the population activity profile (**Fig. 4 h-k,q,r**). The onset of inhibition (**Fig. 2 r,t** and **4 q,r**) was measured as the first 1 ms bin after 0 where the crosscorrelogram was below 3 std of a baseline measured in the preceding 20 ms.

Generalized linear model. We used neuroGLM (https://github.com/pillowlab/neuroGLM.git) to classify neuronal responses with models obtained from linear regression between external covariates and spike trains in single trials. Spike trains were discretized into 1 ms bins and each external event was represented as follows: running speed was added as a continuous variable. Reward times, lick times, and visual cue times were represented as boxcar functions convolved with smooth temporal basis functions defined by raised cosine bumps separated by $\pi/2$ radians (25 ms). The resulting basis functions covered a -4 to 2 s window centred on reward time, and -2 to 2 s windows for lick and visual cue times. We then computed Poisson regression between spike trains and the basis functions and running speed. The resulting weight vectors were then convolved with event times and linearly fitted with the spike times peri-stimulus time histograms smoothed with a 25 ms Gaussian to compute the coefficient of determination for each trial. We divided the fit between reward times model and firing rates in two time windows: -4 to 0 s and 0 to 2s relative to reward time to differentiate between pre- and post-reward neuronal activity. Fits with mean coefficient of determination across trials exceeding 0.1 were selected to classify units.

References

1. Mauk, M. D. & Buonomano, D. V. the Neural Basis of Temporal Processing. *Annu. Rev. Neurosci.* **27,** 307–340 (2004).

2. Leergaard, T. B., Lillehaug, S., De Schutter, E., Bower, J. M. & Bjaalie, J. G. Topographical organization of pathways from somatosensory cortex through the pontine nuclei to tactile regions of the rat cerebellar hemispheres. *Eur. J. Neurosci.* **24,** 2801–2812 (2006).

3. Suzuki, L., Coulon, P., Sabel-Goedknegt, E. H. & Ruigrok, T. J. H. Organization of Cerebral Projections to Identified Cerebellar Zones in the Posterior Cerebellum of the Rat. *J. Neurosci.* **32,** 10854–10869 (2012).

4. Proville, R. D. *et al.* Cerebellum involvement in cortical sensorimotor circuits for the control of voluntary movements. *Nat. Neurosci.* **17,** 1233–1239 (2014).

5. Jörntell, H. & Ekerot, C. F. Topographical organization of projections to cat motor cortex from nucleus interpositus anterior and forelimb skin. *J. Physiol.* **514,** 551–566 (1999).

6. Lu, X., Miyachi, S., Ito, Y., Nambu, A. & Takada, M. Topographic distribution of output neurons in cerebellar nuclei and cortex to somatotopic map of primary motor cortex. *Eur. J. Neurosci.* **25,** 2374–2382 (2007).

7. Person, A. L. & Raman, I. M. Purkinje neuron synchrony elicits time-locked spiking in the cerebellar nuclei. *Nature* **481,** 502–505 (2012).

8. Ichinohe, N., Mori, F. & Shoumura, K. A di-synaptic projection from the lateral cerebellar nucleus to the laterodorsal part of the striatum via the central lateral nucleus of the thalamus in the rat. *Brain Res.* **880,** 191–197 (2000).

9. Sawyer, S. F., Tepper, J. M. & Groves, P. M. Cerebellar-responsive neurons in the thalamic ventroanterior-ventrolateral complex of rats: Light and electron microscopy. *Neuroscience* **63,** 725–745 (1994).

10. Kelly, R. M. & Strick, P. L. Cerebellar loops with motor cortex and prefrontal cortex of a nonhuman primate. *J. Neurosci.* **23,** 8432–8444 (2003).

11. Middleton, F. A. & Strick, P. L. Cerebellar output channels. *Int. Rev. Neurobiol.* **41,** 61–82 (1997).

12. Thach, W. T. & Jones, E. G. The cerebellar dentatothalamic connection: terminal field, lamellae, rods and somatotopy. *Brain Res.* **169,** 168–172 (1979).

13. Huang, C. C. *et al.* Convergence of pontine and proprioceptive streams onto multimodal cerebellar granule cells. *Elife* **2013,** 1–17 (2013).

14. Kennedy, A. *et al.* A temporal basis for predicting the sensory consequences of motor commands in an electric fish. *Nat. Neurosci.* **17,** 416–422 (2014).

15. Wagner, M. J., Hyun Kim, T., Savall, J., Schnitzer, M. J. & Luo, L. Cerebellar granule cells encode the expectation of reward. *Nat. Lett.* 1–18 (2017). doi:10.1038/nature21726

16. Giovannucci, A. *et al.* Cerebellar granule cells acquire a widespread predictive feedback signal

during motor learning. *Nat. Neurosci.* **20,** 727–734 (2017).

17. Ashmore, R. C. & Sommer, M. A. Delay activity of saccade-related neurons in the caudal dentate nucleus of the macaque cerebellum. *J. Neurophysiol.* **109,** 2129–2144 (2013).

18. Ohmae, S., Kunimatsu, J. & Tanaka, M. Cerebellar Roles in Self-Timing for Sub- and Supra-Second Intervals. *J. Neurosci.* **37,** 3511–3522 (2017).

19. Dietrichs, E. The cerebellar corticonuclear and nucleocortical projections in the cat as studied with anterograde and retrograde transport of horseradish peroxidase - V. The posterior lobe vermis and the flocculo-nodular lobe. *Anat. Embryol. (Berl).* **167,** 449–462 (1983).

20. Sun, L. W. Viral and Non-viral Tracing of Cerebellar Corticonuclear and Vestibulorubral Projections in the Mouse. *Open J. Neurosci.* **3,** 1–15 (2013).

21. Park, I. M., Meister, M. L. R., Huk, A. C. & Pillow, J. W. Encoding and decoding in parietal cortex during sensorimotor decision-making. *Nat Neurosci* **17,** 1395–1403 (2014).

22. Svoboda, K. & Li, N. Neural mechanisms of movement planning: motor cortex and beyond. *Curr. Opin. Neurobiol.* **49,** 33–41 (2018).

23. Li, N., Chen, T.-W., Guo, Z. V, Gerfen, C. R. & Svoboda, K. A motor cortex circuit for motor planning and movement. *Nature* **519,** 51–56 (2015).

24. Guo, Z. V. *et al.* Maintenance of persistent activity in a frontal thalamocortical loop. *Nature* **545,** 181–186 (2017).

25. Murakami, M., Vicente, M. I., Costa, G. M. & Mainen, Z. F. Neural antecedents of self-initiated actions in secondary motor cortex. *Nat. Neurosci.* **17,** 1574–1582 (2014).

26. Rickert, J., Riehle, A., Aertsen, A., Rotter, S. & Nawrot, M. P. Dynamic Encoding of Movement Direction in Motor Cortical Neurons. *J. Neurosci.* **29,** 13870–13882 (2009).

27. Reinhold, K., Lien, A. D. & Scanziani, M. Distinct recurrent versus afferent dynamics in cortical visual processing. *Nat. Neurosci.* **18,** (2015).

28. Schmitt, L. I. *et al.* Thalamic amplification of cortical connectivity sustains attentional control. *Nature* **545,** 219–223 (2017).

29. Diener, H. C., Dichgans, J., Guschlbauer, B., Bacher, M. & Langenbach, P. Disturbances of motor preparation in basal ganglia and cerebellar disorders. *Prog. Brain Res.* **80,** 480–481 (1989).

30. Purzner, J. *et al.* Involvement of the Basal Ganglia and Cerebellar Motor Pathways in the Preparation of Self-Initiated and Externally Triggered Movements in Humans. *J. Neurosci.* **27,** 6029–6036 (2007).

31. Perrett, S. P., Ruiz, B. P. & Mauk, M. D. Cerebellar cortex lesions disrupt learning-dependent timing of conditioned eyelid responses. *J. Neurosci.* **13,** 1708–1718 (1993).

32. Kotani, S., Kawahara, S. & Kirino, Y. Purkinje cell activity during learning a new timing in classical eyeblink conditioning. *Brain Res.* **994,** 193–202 (2003).

33. Ramnani, N. The primate cortico-cerebellar system: anatomy and function. *Nat. Rev. Neurosci.* **7,** 511–522 (2006).

34. Habas, C. *et al.* Distinct Cerebellar Contributions to Intrinsic Connectivity Networks. *J. Neurosci.* **29,** 8586–8594 (2009).

35. Baumann, O. *et al.* Consensus Paper: The Role of the Cerebellum in Perceptual Processes. *The Cerebellum* 197–220 (2014). doi:10.1007/s12311-014-0627-7

36. Sokolov, A. A., Miall, R. C. & Ivry, R. B. The Cerebellum: Adaptive Prediction for Movement and Cognition. *Trends Cogn. Sci.* **21,** 313–332 (2017).

37. Strick, P. L., Dum, R. P. & Fiez, J. a. Cerebellum and nonmotor function. *Annu. Rev. Neurosci.* **32,** 413–434 (2009).

38. Pachitariu, M., Steinmetz, N., Kadir, S., Carandini, M. & Harris, K. D. Kilosort: realtime spike-sorting for extracellular electrophysiology with hundreds of channels. *bioRxiv* 61481 (2016). doi:10.1101/061481

39. Guo, Z., Li, N., Huber, D., Ophir, E. & Gutnisky, D. Flow of Cortical Activity Underlying a Tactile Decision in Mice. *Neuron* **81,** 179–194 (2014).

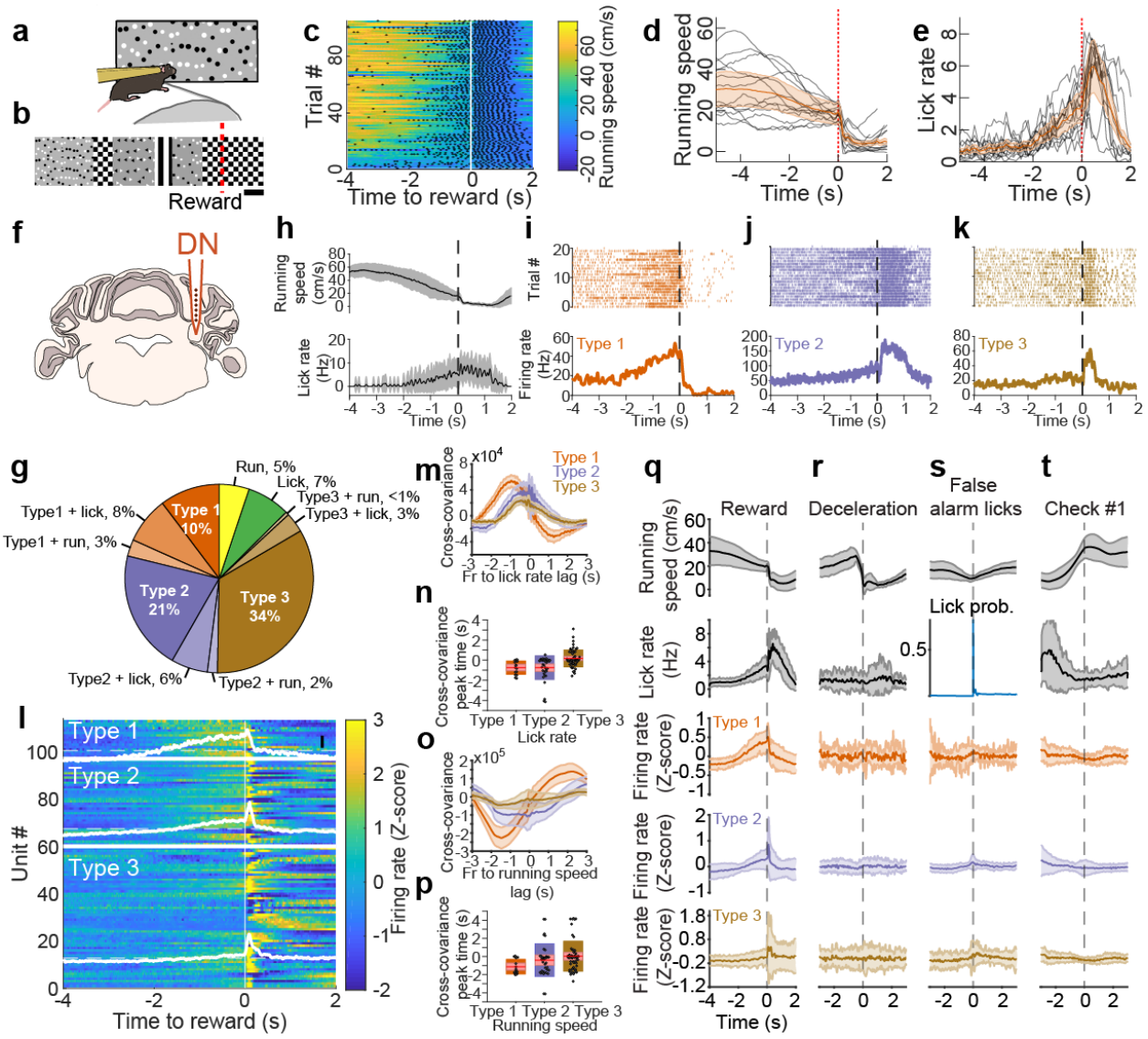

Figure 1 | Preparatory signals in the dentate nucleus. a, Schematic of the virtual reality setup. **B**, Structure of visual textures lining the virtual corridor walls. The scale bar represents a distance of 40 cm. Red dotted line defines the location of reward delivery. **c,** Summary of behavior for an example recording session in a trained mouse. Running speed is color-coded. Black dots represent individual lick times. Reward time is indicated by the vertical white line. **d,** Running speed profiles for all mice (black curves, 13 expert mice) and population average (orange trace, shading is SEM). Red vertical dashed line indicates reward. **e,** Same as **d** but for lick rate. **f,**, Schematic showing recording location in the cerebellar dentate nucleus (DN). **g**, Summary DN neuron classification. **h**, Running speed (top) and lick rate (bottom) around reward time for an example recording. Black line is the average, grey shaded area is the standard deviation. **i-k**, Spiking activity from example neurons in DN, classified as Type 1, Type 2 and Type 3. Top, spike raster for 20 consecutive trials. Bottom, average response profile centered on

447 reward delivery (t = 0 s) from the same trials shown above. The vertical dotted line across **h-k** indicates
448 reward time. **l**, Z-scored firing rate of Type 1, Type 2 and Type 3 DN neurons centered on reward time.
449 White traces represent the average z-scored firing rate within each response type, the black scale bar in
450 the top right corner represents 1 z-score unit. The white vertical line indicates reward time. **m**, Average
451 cross-covariance between firing rates of all neurons (grouped by type) and lick rate for -2 to 2 s time lags
452 (10 ms binning). The shaded areas represent SEM. **n**, Summary of firing rate to lick rate cross-covariance
453 peak times for each neuron, grouped by type. Values of individual neurons are shown as black dots. In
454 box plots, the red line represent the mean cross-covariance peak time value, the pink box represent the
455 SEM and the box color-coded according to neuron type the SD. **o,p**, Cross-covariance between firing
456 rates and running speed, description as in panels **m,n**. **q**, Average (line) and standard deviation (shaded
457 area) of firing rate centered on reward delivery (t = 0 s) for running speed, lick rate, firing rate (z-
458 scored), averaged for all Type 1, Type 2, and Type 3 units. **r-t**, Same as in **q** for responses centered on
459 deceleration events outside of the reward zone, first lick of a train (displayed as lick probability) outside
460 of the reward zone and the appearance of the first non-rewarded checkerboard visual stimulus.
461

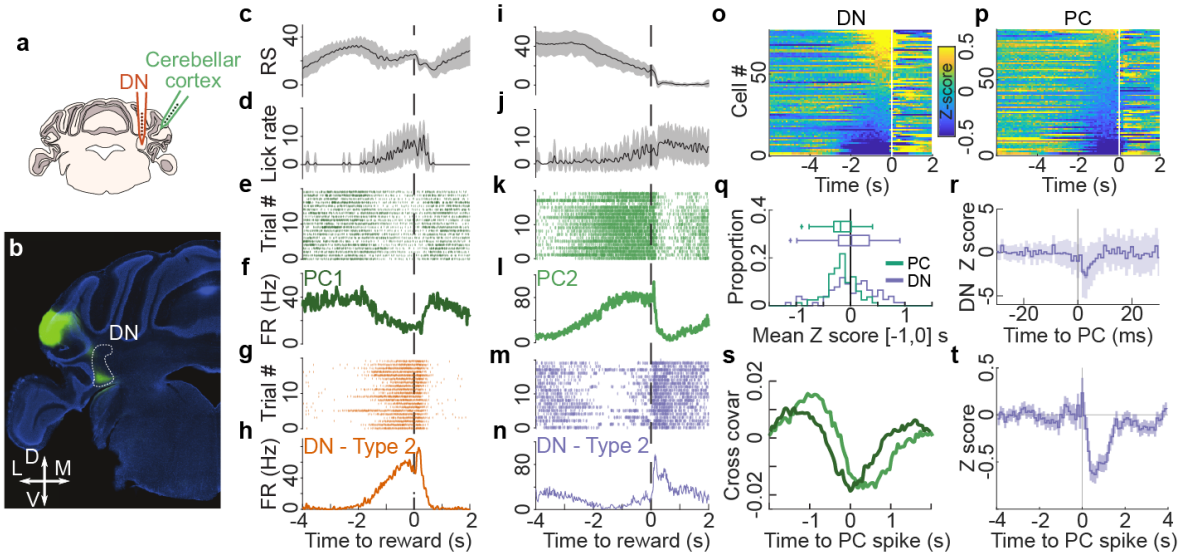

Figure 2 | The relationship between activity of Lateral Crus1 Purkinje cells and dentate neurons. a, Schematic of experiments. The neurons in dentate nucleus (DN, orange) and putative Purkinje cells (PCs) in the cerebellar cortex (green) were simultaneously recorded in mice performing the task. **b,** Injection of AAV expressing GFP in the cerebellar cortex marking the axons of Purkinje cells (PC, green) projecting to the part of the DN (white outline) that was targeted for recordings. Coronal slice, counterstained with DAPI (blue). **c-n,** Examples of simultaneously recorded neurons including a type 1 DN cell (**c-h**) and a type 2 DN cell (**i-n**). Running speed (RS, in Hz, **c,i**), lick rate (in Hz, **d,j**), spike raster plot for PC (**e,k**) and DN neuron (**g,m**) and mean firing rate of the same neurons (**f,l,h,n**) aligned on reward. **o,p,** Average response profiles for all DN neurons (**o**) and all PCs (**p**) sorted by their mean Z score value in the last second before reward. White vertical line indicates reward time. **q,** Distribution (bottom) and bar plot (top) of mean Z-score value in the last second before reward for PC (green) and DN neurons (purple). **r,** Average Z-scored cross-correlogram for all modulated DN-PC pairs (56/2163 pairs, see Methods) showing a short latency inhibition consistent with a monosynaptic inhibitory connection from PCs to DN cells. Line is the mean, dark purple shading is SEM and light shading is std. **s,** Cross-covariance between example PCs and DN cells from panel **c-h** (dark green) and panel **i-n** (light green) at different lags (5ms bins). **t,** Average shuffle-corrected cross-correlogram (see Methods) for all the recorded pairs (n = 2163 pairs, 3 mice) showing a decrease in the probability of DN cell firing in the second following PC activity. Trace is mean +/- SEM.

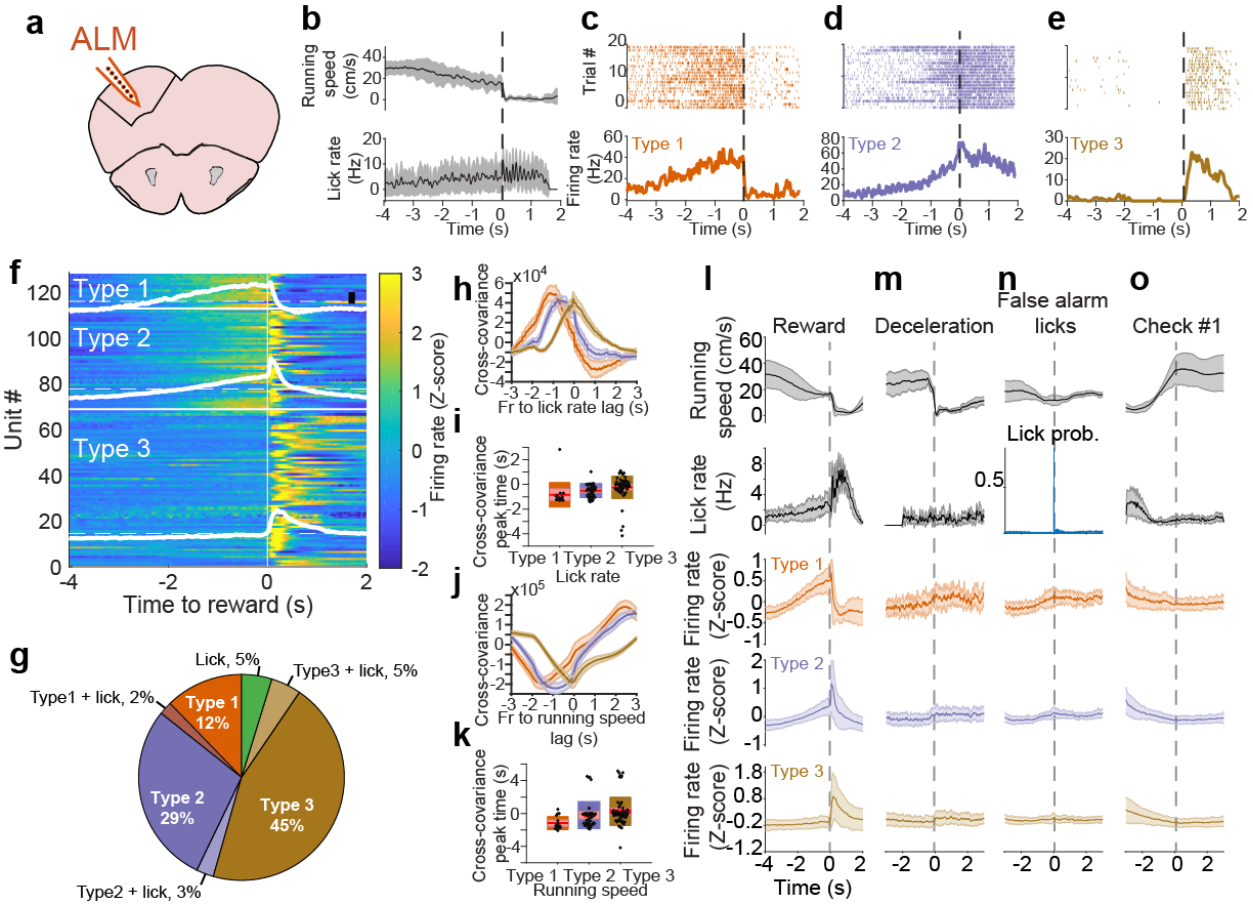

Figure 3 | Preparatory activity in ALM. a, Schematic showing recording location in ALM. **b**, Summary ALM neuron classification. **c**, Running speed (top) and lick rate (bottom) around reward time for an example recording. Black line is the average, grey shaded area is the standard deviation. **d-f**, Spiking activity from example neurons in ALM, classified as Type 1, Type 2 and Type 3. Top, spike raster for 20 consecutive trials. Bottom, average response profile centered on reward delivery (t = 0 s) from the same trials shown above. The vertical dotted line across **c-f** indicates reward time. **g**, Activity of Type 1, Type 2 and Type 3 ALM neurons centered on reward time. White traces represent the average z-scored firing rate within each response type, the black scale bar in the top right corner represents 1 z-score unit. The white vertical line indicates reward time. **h**, Average cross-covariance between firing rates of all neurons (grouped by type) and lick rate for -2 to 2 s time lags (10 ms binning). The shaded areas represent SEM. **i**, Summary of firing rate to lick rate cross-covariance peak times for each neuron grouped by types. Values of individual neurons are shown as black dots. In box plots, the red line represent the mean cross-covariance peak time value, the pink box represent the SEM and the box color-coded according to neuron type the SD. **j,k**, Cross-covariance between firing rates and running speed, description as in panels **h,i**. **l**, Average (line) and standard deviation (shaded area) of firing rate centered on reward

499 delivery (t = 0 s) for running speed, lick rate, firing rate (z-scored), averaged for all Type 1, Type 2, and
500 Type 3 units. **m-o**, Same as in **l** for responses centered on deceleration events outside of the reward
501 zone, first lick of a train (displayed as lick probability) outside of the reward zone and the appearance of
502 the first non-rewarded checkerboard visual stimulus.
503

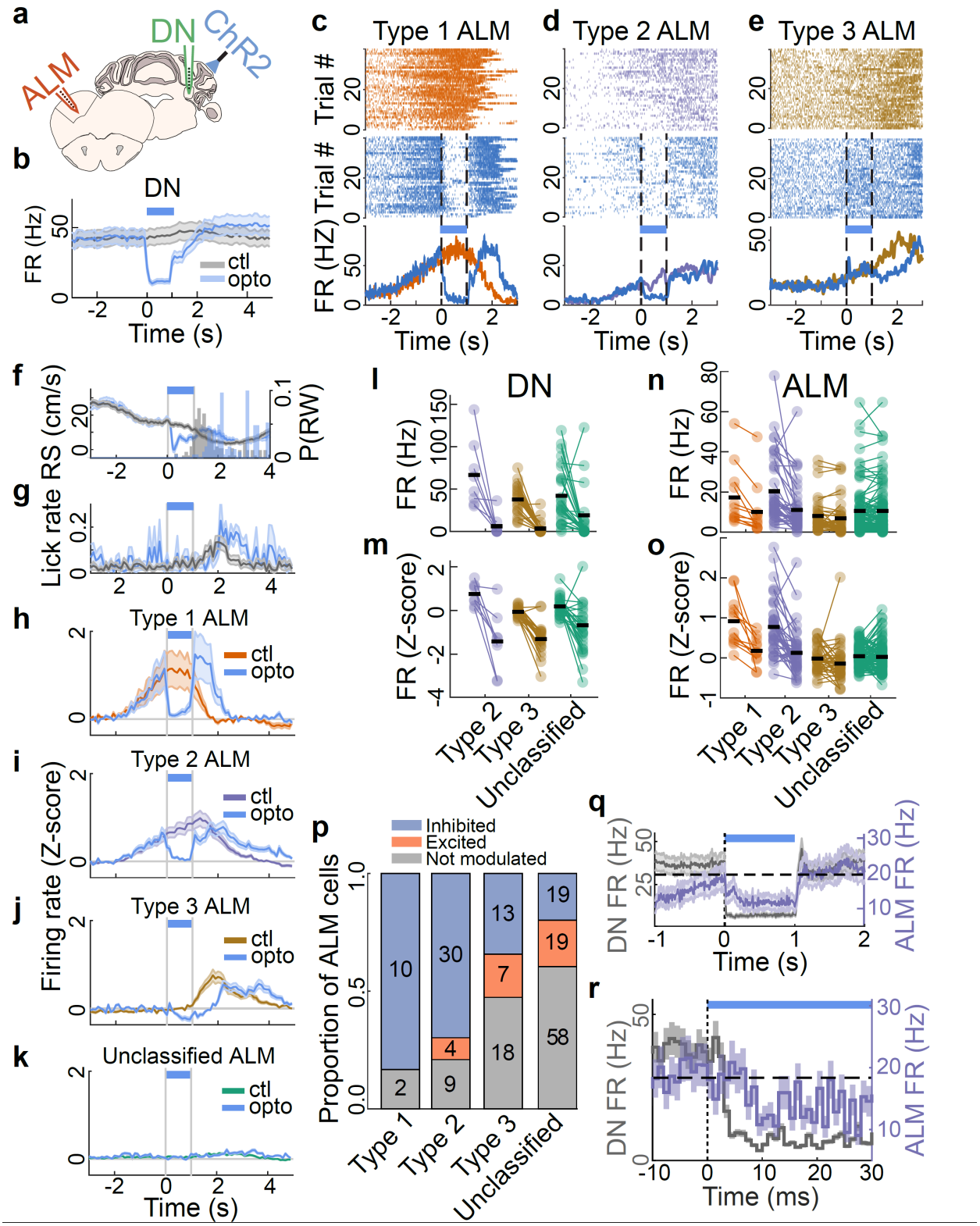

Figure 4 | Cerebellar output is required for the persistence of ALM preparatory activity. a, Schematic of experiments. The DN (green) and ALM (orange) were simultaneously recorded in L7-ChR2 mice preforming the task during photoactivation of Purkinje cells (PCs). **b,** PC photoactivation effectively

508 silenced DN population activity. **c-e**, Raster plot during control trials (top) and photoactivation trials
509 (middle), and average responses (bottom) from example neurons recoded in ALM classified as Type 1
510 (**c**), Type 2 (**d**) or Type 3 (**e**). **f-g,** Average profiles around time of stimulation in photoactivation trials
511 (blue lines) and control trials (grey lines) for running speed (RS, **f**) and lick rate (**g**), and distribution of
512 reward probability (P(RW)) in photoactivation trials (**f,** blue histogram) and control trials (**f,** grey
513 histogram). **h-k**, Response profiles of ALM neurons aligned to photoactivation onset for Type 1 (**h**), Type
514 2 (**i**), Type 3 (**j**) and unclassified cells (**k**) during photoactivation (blue traces) and control trials (coloured
515 traces). **l-o**. Quantification of modulation. Average firing rate (**l,n**) and z-scored firing rate (**m,o**) during
516 the first second after stimulation time for DN neurons (**l,m**) and ALM neurons (**n,o**). For all plots the first
517 column of dots (one per cell) is the control condition, the second column the photoactivation condition.
518 The black lines indicate the population mean. All types of DN cells were inhibited by photoactivation
519 (**l,m**) while only Type 1 and 2 ALM cells showed a significant inhibition (**n,o**). **p**. Proportion of cells being
520 inhibited (blue), excited (red) or not significantly modulated (grey) for the 4 classes of neurons (number
521 of cells indicated in each bar). **q,r.** Average response profiles of firing rate around PC photostimulation
522 onset for all DN neurons (grey) and all Type 1 and Type 2 ALM neurons (purple). Short-latency
523 suppression persisted for 1 second, followed by a small rebound (**q**, 10ms bins, **r**, 1ms bins). In all plots,
524 curves with shaded areas are mean +/- sem.**,** Schematic of experiments. The DN (green) and ALM
525 (orange) were simultaneously recorded in L7-ChR2 mice preforming the task during photoactivation of
526 Purkinje cells (PCs).
527

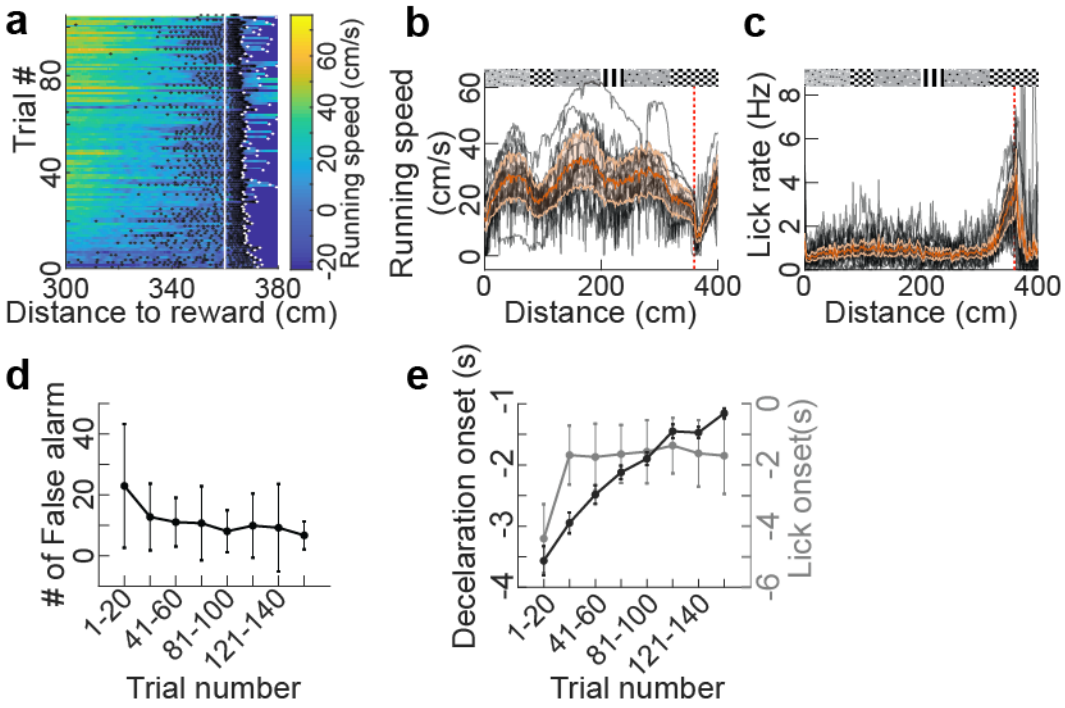

Extended data figure 1 (attached to Fig. 1) | Refinement of motor behaviour in anticipation of reward. **a,** Summary of behavior for an example recording session of a trained mouse. Running speed over distance is color-coded. Black and white dots represent individual lick times and end of trial, respectively. Reward time is indicated by the vertical white line. **b,** Running speed profiles for all mice (black curves, 13 expert mice) and population average (orange trace, shading is SEM) aligned on distance to the reward. Red vertical dashed line indicates reward. **c**, Same as **b** but for lick rate. **d**, Number of false alarm licks averaged in chunks of 20 trials over the course of recording sessions across all mice. Error bars are standard deviations. **e**, Summary plots of deceleration and lick rate onsets relative to reward time (respectively, onset of 20% decrease and increase of Z-score values) averaged in chunks of 20 trials across recording sessions. Error bars are standard deviations.

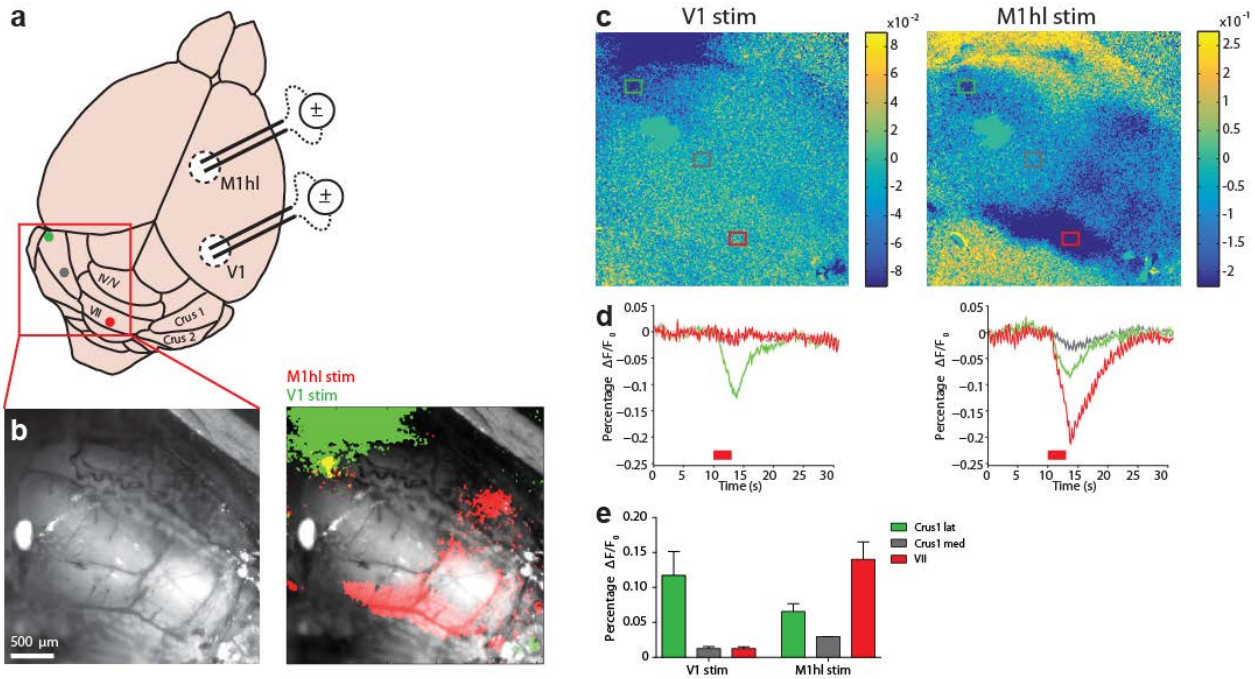

Extended data figure 2 (attached to Fig. 2 and 3) | Mapping visuomotor cerebellum. a, Schematic of electrical stimulation for identification of a cerebellar region activated by inputs from primary visual cortex (V1) and hind limb-related motor cortex (M1hl). Coloured dots correspond to regions from where hemodynamic signals were measured in **c-e**: lateral crus1, medial crus 1 and lobule VII. **b**, Left: wide-field image of the cerebellar surface. Right: same image overlaid with 20-trials average of hemodynamic signals averaged across sessions (showing only peak decrease from baseline) for electrical stimulation of V1 (green) and M1hl (red). **c**, Wide-field image of 20-trials average hemodynamic signals color-coded according to percentage change of infrared (IR) reflectance from baseline for V1 (left) and M1hl stimulation (right). Coloured rectangles indicate the areas from which the signals were measured from. **d**, Mean response time courses after V1 (left) and M1hl stimulation (right) color-coded according to the sampled areas in **c**. ΔF/F0, normalized change in reflectance. The timing of electrical stimulation is indicated by the red bar below the traces. **e**, Summary of peak hemodynamic response values after V1 (left) and M1hl (right) stimulations for each cerebellar area.

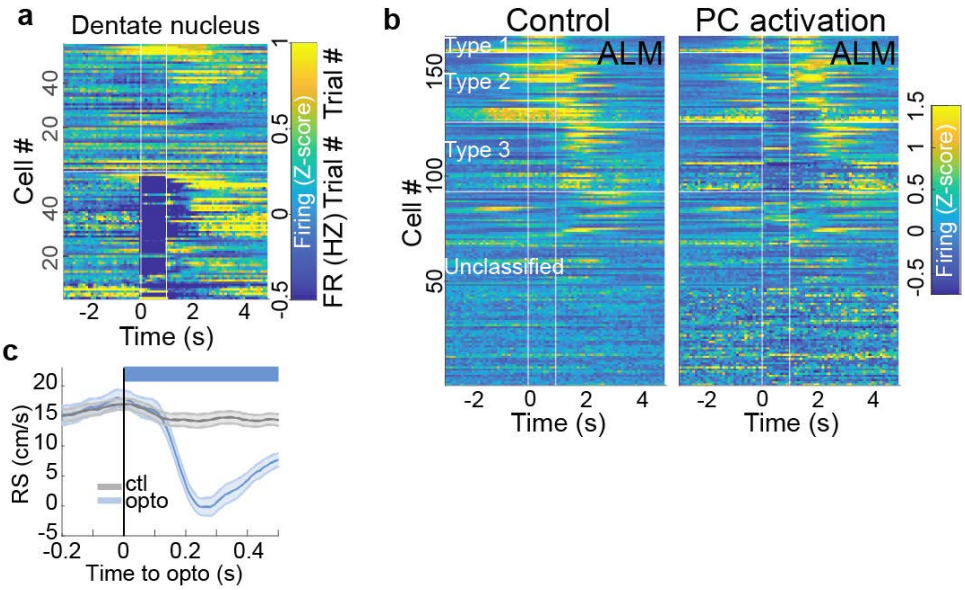

559

560 **Extended data figure 3 (attached to Fig 4) | Effects of cerebellar Purkinje cells photoactivation on DN**
561 **and ALM neuronal populations and on mouse locomotion.a,** Purkinje cell (PC) photoactivation
562 efficiently inhibited most DN neurons (one line per neuron). Upper half: control trials. Lower half:
563 photoactivation trials. **b**, Purkinje cell photoactivation efficiently suppressed activity in most type 1 and
564 type 2 ALM neurons (one line per neuron). Purkinje cell photoactivation (right) compared to control
565 trials (left). The effects of photoactivation on Type 3 and unclassified ALM cells were more diverse. **c**,
566 The effect on PC photoactivation ('opto') on running speed (RS).

567

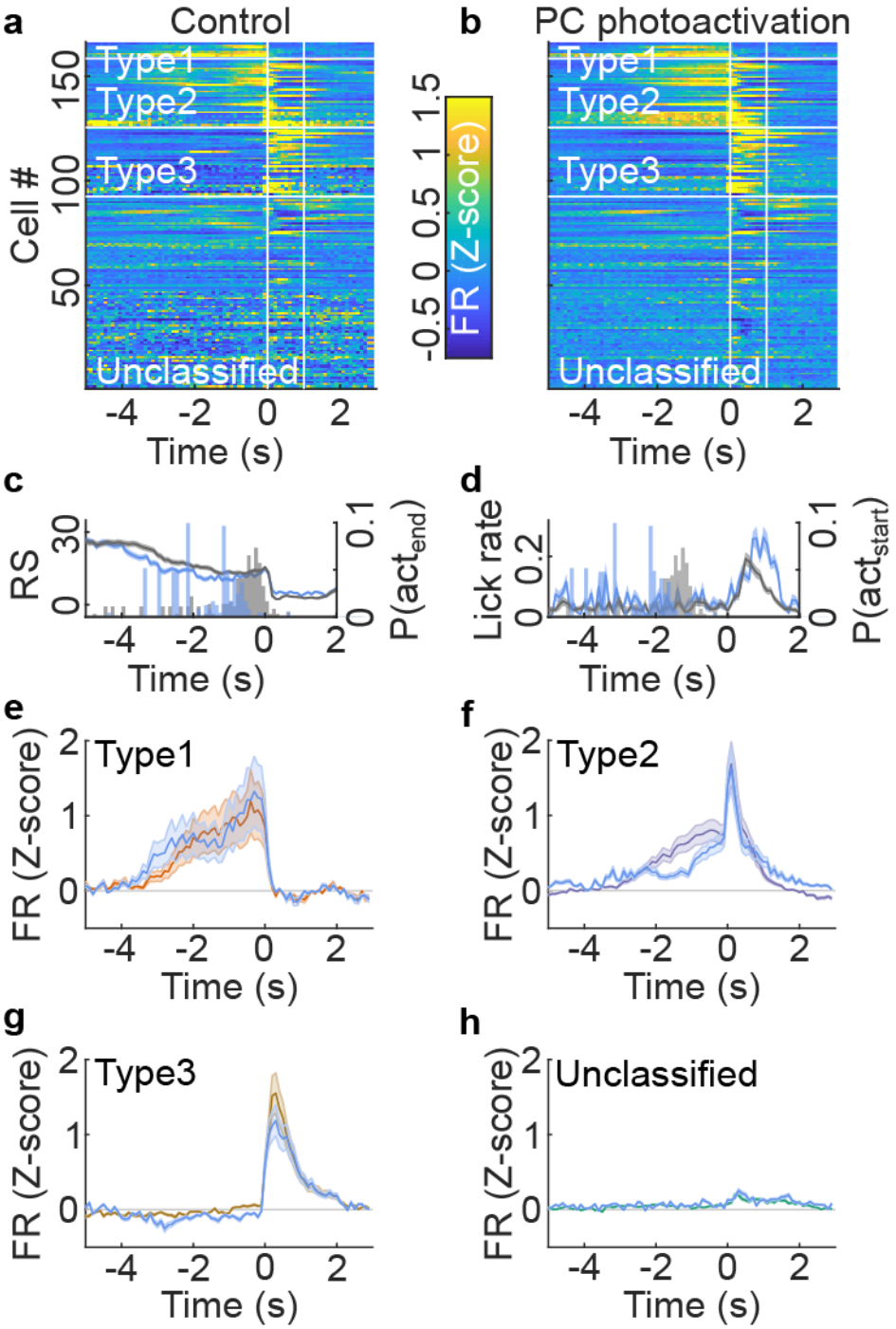

Extended data figure 4 (attached to Fig 4) | Effects of cerebellar photoactivation on ALM activity aligned to reward time. a,b, Response profiles colour coded by firing rate z-score for all ALM neurons sorted by cell type in control condition (**a**) and with photoactivation of Purkinje cells (PC, **b**) aligned on time of reward delivery. **c,d**, Average profiles around time of stimulation in photoactivation trials (blue lines) and control trials (grey lines) for running speed (RS, **c**) and lick rate (**d**). Histograms indicate the

574 start (**d**) and end (**c**) of the photoactivation period in control (gray) and test trials (blue). **e-h**, Firing rate
575 profiles aligned to reward time for Type 1 (**e**), Type 2 (**f**), Type 3 (**g**) and unclassified ALM neurons (**h**)
576 during photoactivation (blue traces) and control trials (coloured traces).